Avalanche dynamics of ferroelectric phase transitions in BaTiO$_3$ and 0.7Pb(Mg$_{2/3}$Nb$_{1/3}$)O$_3$-0.3PbTiO$_3$ single crystals

Yangyang Xu, Dezhen Xue (iD), Yumei Zhou, Tong Su, Xiangdong Ding (iD), Jun Sun, and E. K. H. Salje

View Online   Export Citation   CrossMark

ARTICLES YOU MAY BE INTERESTED IN

Avalanche dynamics of ferroelectric phase transitions in BaTiO₃ and 0.7Pb(Mg2/3Nb1/3)O₃-0.3PbTiO₃ single crystals

Yangyang Xu,[1] Dezhen Xue,[1,a)] (ID) Yumei Zhou,[1,b)] Tong Su,[1] Xiangdong Ding,[1] (ID) Jun Sun,[1] and E. K. H. Salje[1,2]

AFFILIATIONS

[1]State Key Laboratory for Mechanical Behavior of Materials, Xian Jiaotong University, Xian 710049, China
[2]Department of Earth Sciences, Cambridge University, Downing Street, Cambridge CB2 3EQ, United Kingdom

[a)]Electronic mail: xuedezhen@xjtu.edu.cn
[b)]Electronic mail: zhouyumei@xjtu.edu.cn

ABSTRACT

The motion of phase fronts during a ferroelectric phase transition is intermittent and follows avalanche dynamics. In the present study, we show that an intermittent propagation mode generates spikes of depolarization currents at an extremely slow heating rate of 0.05 K/min in BaTiO₃ (BTO) and 0.7Pb(Mg2/3Nb1/3)O₃-0.3PbTiO₃ (PMN-PT) single crystals. Such "jerks" are indicative of avalanche dynamics, and their energy exhibits a power law distribution with exponents of $\varepsilon = 1.3 \pm 0.10$ and $\varepsilon = 1.5 \pm 0.10$ for BTO and PMN-PT, respectively. The rate of aftershocks after big events decays as an Omori-like power-law and interevent times are characterized by a universal double power-law distribution, indicating the critical temporal correlations between the avalanche events.

Published under license by AIP Publishing. https://doi.org/10.1063/1.5099212

Ferroelectrics undergo a centrosymmetric-to-polar structural phase transition upon cooling.[1] The symmetry-lowering transition generates, in most cases, complex domain patterns in the low temperature ferroelectric phase.[1] The domains are switchable under electric and/or mechanical fields, which defines the ferroic hysteresis and is always fundamental to a vast spectrum of applications, including ultrasonic transducers, precision actuators, and nonvolatile memories.[1–3] Most applications are directly related to the features of domains, such as the morphology and density, which are produced and controlled by the symmetry-lowering ferroelectric phase transition.[1,2] Efforts have been devoted to studying the equilibrium properties of the ferroelectric phase transition, such as the origin of ferroelectricity, and the effects of the pressure, size, strain, and defect on the transition behaviors,[4–11] while we focus on its dynamics here.

The ferroelectric phase transitions are of first order in many of the ferroelectric materials.[1,10] Thus, there exists an invariant interphase boundary, i.e., a phase front, which separates the high symmetry paraelectric and low symmetry ferroelectric phases during the transition. The behavior of the phase front is regarded as being athermal, and the propagation can only occur under the change of temperature (or the application of external field), which modifies the free energy difference between high and low symmetry phases.[12,13] The behavior is in contrast to thermally activated transitions during which the relaxation between different states takes place at constant external conditions due to thermal fluctuations. In ferroelectric materials, we find structural disorder, including self-generated domain walls and their intersections by long-range electric and elastic interactions, and the intrinsic defects such as dopants, vacancies, dislocations, grain boundaries, and local composition fluctuations.[14] The phase front strongly interacts with disorder during the ferroelectric phase transition so that a smooth, fully continuous propagation of the phase front rarely exists. Consequently, the transition proceeds through a set of metastable states of free energy local minima, leading to intermittent and discrete avalanches.[15]

Similar avalanche events have been found during earth quakes,[16] the plastic deformation of solids,[17,18] the failure of materials,[19] the condensation,[20] the switching processes of magnetization and polarization,[21–24] and structural phase transitions.[25] Avalanches show the absence of characteristic scales, which reveals the existence of a certain kind of criticality.[26] The probability density $P(E)$ of an avalanche with energy of E is usually displayed by the power law distribution $P(E) \sim E^{-\varepsilon} F(E)$, where $F(E)$ is a certain (exponential) cut-off function.[27] Besides the size of the events, they exhibit critical temporal clustering correlations as well, which follow similar power law distributions.[15]

Acoustic emission (AE) has been employed to detect the acoustic waves in the range from kilohertz to megahertz which are due to sudden strain changes at the propagating interfaces during the ferroelectric phase transition.[28–30] The AE signals carry the whole temporal and spatial information of the ferroelectric transitions (strictly speaking, the ferroelastic transitions).[23,25,31] Calorimetry with a very high signal and time resolution can also potentially be utilized to probe the avalanche dynamics of the ferroelectric phase transition.[15,32] However, both techniques detect the signal originating from the slave order parameters of the ferroelectric transitions, such as strain and thermal properties. As the polarization is the primary order parameter, a direct measurement of electric signals from polarization is of importance to study the dynamics of ferroelectric phase transition.

In the present study, we employed a high-precision thermally stimulated depolarization current (TSDC) measurement to investigate the avalanche dynamics during ferroelectric phase transition by monitoring the primary order parameter change. Our samples are single crystals of BaTiO$_3$ (BTO) and 0.7Pb(Mg$_{2/3}$Nb$_{1/3}$)O$_3$-0.3PbTiO$_3$ (PMN-PT) with different orientations.[33–35] The sample details are listed in Table S1 of the supplementary material. The top and bottom surfaces were covered with silver electrodes. Thermally stimulated depolarization current (TSDC) analysis was undertaken in a Linkam THMS600 temperature stage with temperature scans as slow as 0.01 K/min. The depolarization current was measured using a high resistance electrometer Keithley 6517B. The typical experimental protocol is as follows: before the TSDC measurement, all samples were depoled at 473 K for 30 min. This thermal treatment also released unwanted heterogeneous stress fields. The samples were then poled with a field of 10 KV/cm for 5 min at room temperature and heated with rates of 10 K/min, 0.1 K/min, and 0.05 K/min. The data acquisition frequency was 50 Hz. The BTO samples undergo a typical first order ferroelectric phase transition and PMN-PT single crystals possess features of the relaxor ferroelectric transition, as shown by the dielectric, ferroelectric, and thermal characterization in the supplementary material.

Individual avalanches occur on a very short time scale. When the phase transition is driven too fast, the change of the order parameter always looks continuous, as various events would superpose. Decreasing the heating rate renders individual avalanche events observable. Such slow field/temperature rates were identified as a stringent prerequisite for avalanche studies.[14] To this end, we changed our heating rate from 20 K/min to 0.05 K/min step by step. Typical TSDC curves for three different heating rates of 10 K/min, 0.1 K/min, and 0.05 K/min are shown in Fig. 1.

Only a main pyroelectric current peak in Fig. 1(a) can be observed for a fast heating rate of 10 K/min in BTO ⟨100⟩, corresponding to the ferroelectric to paraelectric phase transition. With the decreasing heating rate to 0.1 K/min, the pyroelectric current peak in Fig. 1(a) splits into several peaks with a reduction of the magnitude of the peaks by one order of magnitude compared with the fast heating rate. The number of current spikes is still small, and the overlap of events is likely to happen. At an even lower heating rate to 0.05 K/min, the TSDC detects more than 1000 spikes, as shown in Fig. 1(a). These data allow a fairly reliable statistical analysis even though the magnitude of large spikes is now one order lower than that of 0.1 K/min. Figure 1(c) shows that the TSDC in PMN-PT has a similar tendency to BTO: the magnitude of current spikes drops, but the number increases with the decreasing heating rate. We chose the data with a heating rate of 0.05 K/min for
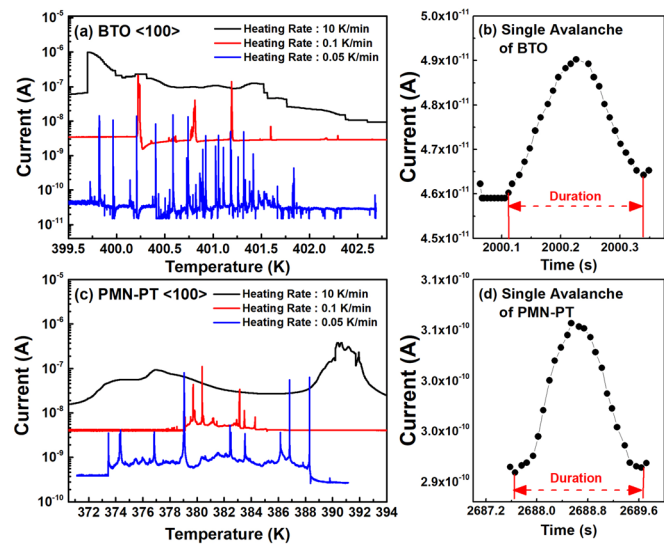

FIG. 1. Spikes of thermally stimulated depolarization current during the phase transformation of (a) BTO and (c) PMN-PT single crystals with an orientation of ⟨100⟩ at three different heating rates. The heating rates are 10 K/min, 0.1 K/min, and 0.05 K/min. Avalanches are shown as individual spikes with the decreasing heating rate. A single avalanche event in an enlarged scale is shown in (b) for BTO and (d) for PMN-PT.

further analysis. The spikes of the experiments were extracted after the removal of a fitted smooth background. As shown in the supplementary material, the noise level of our measurement is below 10^{-11} A. Since almost all our avalanche spikes are larger than this noise level, they do not mix with noise artifacts.

We estimate the energy probability density function (PDF) of avalanches by equating the energy E for each avalanche with $E = I^2 \Delta t R$, where I is the pyroelectric current, Δt is the duration of each avalanche, and R is the resistance of the sample. We consider R as a constant during our measurement so that $E \propto I^2 \Delta t$. The duration has been measured for each jerk signal, and E was determined by this approximation (rather than by integration). The duration of the jerks is shown in the supplementary material. It is heavily curtailed by higher and lower cutoffs. Alternatively, the distribution of the peak intensities without time integration was discussed in the mean field limit by LeBlanc et al. who showed that the effective exponent is higher than the mean field value (3/2 for our case).[36] This value depends on the rate of the measurement and is lowered when the rate is increased. In our experiment, we find an exponent ∼4/3 for BTO after multiplication with the duration so that we take this value as a good approximation of the true energy exponent. We then performed the following statistical analysis of $I^2 \Delta t$ for different samples.

Figure 2(a) shows histograms of the probability densities of energy $P(I^2 \Delta t)$ for BTO single crystals with three orientations ⟨100⟩, ⟨001⟩, and ⟨111⟩ on a log-log scale. All three distributions show a power-law behavior, $P(I^2 \Delta t) \sim (I^2 \Delta t)^{-\varepsilon}$, with the same exponent, which is known as the Gutenberg-Richter law.[37] The power law extends over four to five decades in the measurements with a heating rate of 0.05 K/min. The exponents were further analyzed using a maximum likelihood (ML) method, as shown in Fig. 2(b).[38] We fitted the
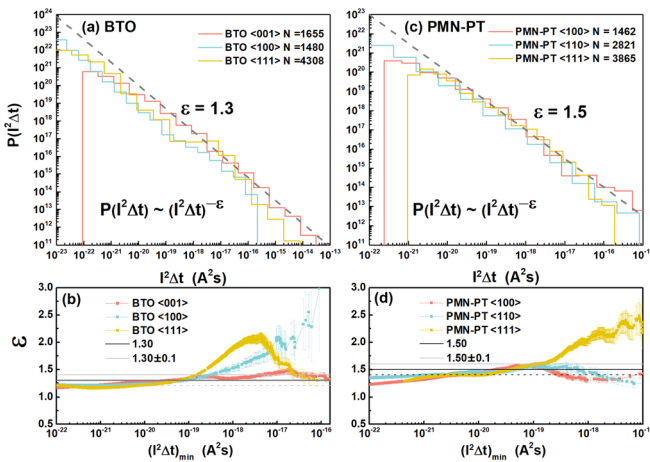
FIG. 2. (a) and (c) Histogram showing the energy distribution (on a log-log scale, with logarithmic binning) for BTO and PMN-PT single crystals with different crystal orientations. The value N is the total number of events detected for each sample. The dashed line corresponds to the power-law probability density function of $P(I^2 \Delta t) \sim (I^2 \Delta t)^{-\varepsilon}$ with $\varepsilon = 1.30$ in (a) and $\varepsilon = 1.50$ in (c). (b) and (d) Maximum likelihood estimate of the exponent ε as a function of a moving minimum energy cutoff, $(I^2 \Delta t)_{min}$. Horizontal lines indicate the values $\varepsilon = 1.30 \pm 0.10$ in (b) and $\varepsilon = 1.50 \pm 0.10$ in (d).

exponent as a function of a lower cutoff, $(I^2 \Delta t)_{min}$, with an assumption that the distribution follows a pure power law behavior.[38] The characteristic exponent was identified by the plateau in the ML plot. For BTO crystals, the estimated exponent ε is 1.30 ± 0.10. A line with a slope of 1.30 is also shown in Fig. 2(a). Figure 2(c) shows the PDF of the energy for PMN-PT single crystals with three orientations $\langle 100 \rangle$, $\langle 110 \rangle$, and $\langle 111 \rangle$. The PDFs are power law distributed and extend over four to five decades. A ML plateau determines the critical exponent for PMN-PT single crystals with ε equal to 1.50 ± 0.10 [Fig. 2(d)].

The size of avalanche events follows a power law distribution at the phase transition point, but there is a difference in the exponent for BTO and PMN-PT single crystals. The exponent 1.30 ± 0.10 of BTO is very close to 1.33 as predicted by mean field theory.[14,18] This fact indicates that the long-range electric and elastic interaction is significant at the ferroelectric transition point. Similarly, phase front propagation during the martensitic transformation in some shape memory alloys has been found to exhibit power-law distribution in equivalent energy of avalanche events with an exponent of 1.3.[14] There is a slight increase in the exponent of PMN-PT to 1.5 ± 0.10. The increment can be ascribed to the higher level of disorders in PMN-PT such as the chemical and charge heterogeneities. The interaction between the phase front and the disorders leads to smaller events, resulting in a larger exponent. The field induced mean field value is 1.66,[14] which was also found for the electric field induced switching in BTO[23] and PZT.[24]

These avalanche events can also be temporally correlated. A simple picture is that the nucleation of the paraelectric cubic phase and its growth affect the occurrence of the coming nucleation or propagation of phase front due to the long-range electric and elastic interactions. We now analyze the distribution of waiting times (interevent times) between consecutive events to test the existence of correlations in time. The waiting time is defined as the time interval between successive events, $\delta_i = t_{i+1} - t_i$, $(i = 1, 2, \ldots)$. Studies on the earthquakes have

shown that the probability density $P(\delta)$ for waiting times (δ_i) above different energy thresholds is normalized by the renormalized function $\Phi(x)$, $P(\delta) = \frac{1}{\langle \delta \rangle} \Phi(\frac{\delta}{\langle \delta \rangle})$, where time is rescaled by the rate of events $\langle \delta \rangle$. $\Phi(x)$ has a form of double power law for the extreme values of x,

$$\Phi(x) = \begin{cases} x^{-(1-\phi)}, & x \ll 1 \\ x^{-(2+\psi)}, & x \gg 1. \end{cases}$$

Such double power-law distributions have been found previously for avalanches during earthquake, fractures of porous materials, and martensitic transformation in shape memory alloys.[14,19,39]

We chose different thresholds on I^2_{min} and only considered the events with I^2 larger than a given I^2_{min}. The scaled waiting time probability densities, $P(\delta, (I^2)_{min})/\langle \delta \rangle$, for different thresholds of various BTO samples are plotted in Fig. 3(a). The short-time range displays a power-law decay with exponent $(1 - \phi) = 1.05 \pm 0.05$, which corresponds to the Omori law. A second power law is observed for the tail of the distribution with an exponent $(2 + \psi) = 2.30 \pm 0.10$. The power law distribution implies the temporal correction between avalanche events. Figure 3(b) shows the scaled probability densities as a function of scaled waiting times for different $(I^2)_{min}$ in different PMN-PT single crystals. The same double power-law distribution was observed, with very similar exponents to those for BTO: $(1 - \phi) = 1.03 \pm 0.05$, $(2 + \psi) = 2.05 \pm 0.10$. Similar values were reported for the epidemic-type aftershock sequence (ETAS) model, earthquakes, and collapsing porous silicon dioxide.[19,39,40]

We now analyze whether the large avalanches induce aftershocks (ASs) and compare the distribution of aftershocks with the Omori law from seismology. This is another test for the time-correlation between events. We considered the events with energies within a certain energy interval as main-shocks (MSs) and smaller, subsequent events after a MS as aftershocks (ASs). A sequence of ASs ends when an event with an energy larger than the energy of the MS is found. We count the
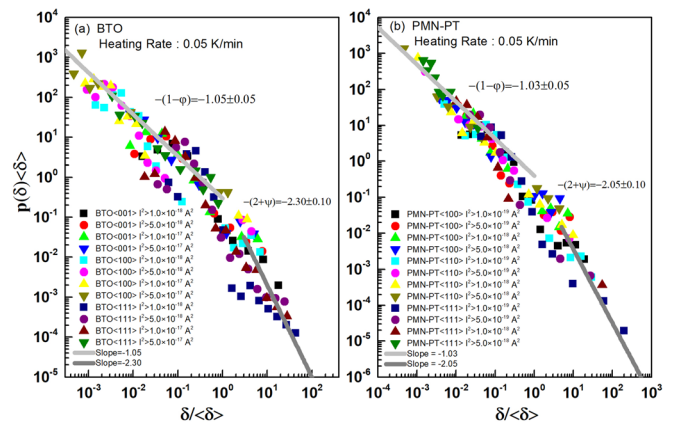

FIG. 3. Collapse of the distribution of rescaled waiting times of (a) BTO and (b) PMN-PT single crystals with different orientations according to the unified scaling law hypothesis. Probability densities of waiting time after rescaling by the mean waiting time $\langle \delta \rangle$. $\langle \delta \rangle$ is calculated by $\langle \delta \rangle = t/N_{(I^2) > (I^2)_{min}}$, where t is the duration time of test and $N_{(I^2) > (I^2)_{min}}$ is the number of events with I^2 above the threshold $((I^2)_{min})$. The time spans five decades. Small waiting times follow a power law distribution with exponents of $(1 - \phi) = 1.05 \pm 0.05$ for BTO and $(1 - \phi) = 1.03 \pm 0.05$ for PMN-PT, while large waiting times has an exponent of $(2 + \psi) = 2.30 \pm 0.10$ for BTO and $(2 + \psi) = 2.05 \pm 0.10$ for PMN-PT.

number of AS within each predivided time interval after a MS. An activity rate of AS, r_{AS}, is then calculated by averaging different sequences of AS corresponding to all MS in the same energy range and then dividing by the number of sequences. Thus, r_{AS} is the number of events per time interval. r_{AS} as a function of time has been shown to follow a power law, namely, the Omori law

$$r_{AS}(t - t_{MS}) = (c - t - t_{MS})^{-p}, \qquad (1)$$

where c is a constant independent of time, and p is a critical exponent near 1 for earthquakes, martensitic transformation in shape memory alloys, and collapsing porous materials.[41,42]

We then plot $r_{AS}(t - t_{MS})$ as a function of time [Fig. 4(a)] for BTO single crystals. For events with the time distance to MS smaller than 10 s, $(t - t_{MS}) < 10$ s, $r_{AS}(t - t_{MS})$ follows the Omori law with an exponent of $p = 1.0 \pm 0.1$. For those with $(t - t_{MS}) > 10$ s, the Omori law is badly defined. Moreover, the larger the energy interval to define MS is, the more the deviations from the Omori law occur. Figure 4(b) shows $r_{AS}(t - t_{MS})$ as a function of time for PMN-PT crystals. It has very similar tendencies to BTO with an Omori exponent close to 1.0. The deviations from the Omori law show that the time correlation of aftershocks is valid for time delays shorter than 10 s. For longer delay times, the "aftershocks" are independent of the MS. The Omori exponent of $p = 1.0 \pm 0.1$ is very close to the value found for collapsing sandstone, coal, and earthquakes.[41,42] These facts indicate that during the ferroelectric transition, the events that occur shortly after a mainshock are strongly correlated, while later events are not.

In summary, we employed thermally stimulated depolarization current (TSDC) measurement to analyze the avalanche behavior of the ferroelectric phase transition in $BaTiO_3$ and $0.7Pb(Mg_{2/3}Nb_{1/3})O_3$-$0.3PbTiO_3$ single crystals. An intermittent transition process can be probed in extremely slow measurements with a heating rate of 0.05 K/min, and each avalanche leads to a jerk in the current spectrum. The jerky spikes are as a result of the sudden changes of the local polarization, being analogous to the Barkhausen noise in magnetic materials, which is associated with changes of magnetization. Their statistical

analysis shows power law scaling of the energy distribution with exponent of $\varepsilon = 1.3 \pm 0.10$ for BTO and $\varepsilon = 1.5 \pm 0.10$ for PMN-PT. The power-law covers 4–5 decades, indicating a lack of characteristic scale for the events of ferroelectric transition. It can be understood as a consequence of a self-organization of the disorder in the sample into a critical state, similar to the situation during the martensitic transformation. The difference in the critical exponent between BTO and PMN-PT could be attributed to different levels of disorders in the two types of crystals. Both energy exponents are close to the mean field value of 1.33 and below the field integrated value of 1.66.[14] Field integrated exponents were recently found for ferroelectric switching in BTO at room temperature (1.65)[23] and slightly lower values near 1.5 for field switching in the Lead Zirconate Titanate (PZT).[24]

Temporal correlations between avalanches during the ferroelectric transitions equally follow mean field predictions. The rate of aftershocks after big events decays as an Omori-like power-law and distribution of waiting times is characterized by a double power-law distribution with exponents close to those observed by Baró et al.[19] During the ferroelectric transition, the Omori law only holds for events with delay times below 10 s, indicating that small events are Omori-like correlated but large events are temporally independent. In addition, the TSDC is quite sensitive to the local change of polarization and can be used to study the switching process and transition in other ferroelectric and multiferroic systems at a slow driven rate.

See the supplementary material for sample information and dielectric, ferroelectric. and thermal characterization of the samples.
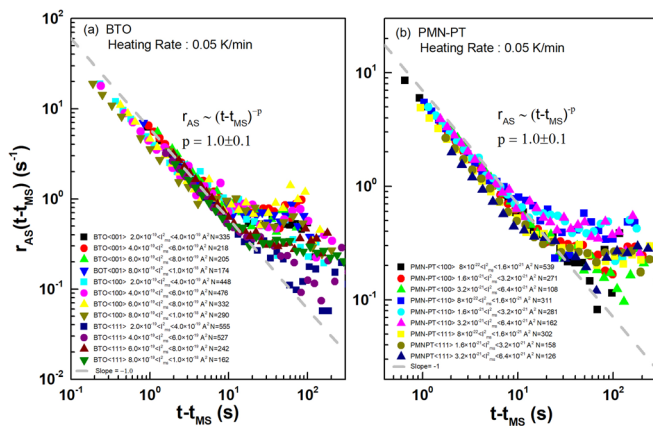
FIG. 4. Activity rate of aftershocks, r_{AS}, as a function of the time distance to the main shock of (a) BTO and (b) PMN-PT single crystal with different orientations. MSs are defined as the events with energies in the range indicated by the legend. N values indicate the number of sequences analyzed for each range. The dashed line indicates the Omori law with a critical exponent of $p = 1.0 \pm 0.1$.

REFERENCES

[1] M. E. Lines and A. M. Glass, *Principles and Applications of Ferroelectrics and Related Materials* (Oxford University Press, 2001).
[2] K. Uchino, *Ferroelectric Devices*, 2nd ed. (CRC Press, 2009).
[3] J. F. Scott, Science **315**, 954 (2007).
[4] R. E. Cohen, Nature **358**, 136 (1992).
[5] W. Zhong, D. Vanderbilt, and K. M. Rabe, Phys. Rev. B **52**, 6301 (1995).
[6] M. Ahart, M. Somayazulu, R. E. Cohen, P. Ganesh, P. Dera, H.-K. Mao, R. J. Hemley, Y. Ren, P. Liermann, and Z. Wu, Nature **451**, 545 (2008).
[7] J. E. Spanier, A. M. Kolpak, J. J. Urban, I. Grinberg, L. Ouyang, W. S. Yun, A. M. Rappe, and H. Park, Nano Lett. **6**, 735 (2006).
[8] J. H. Haeni, P. Irvin, W. Chang, R. Uecker, P. Reiche, Y. L. Li, S. Choudhury, W. Tian, M. E. Hawley, B. Craigo, A. K. Tagantsev, X. Q. Pan, S. K. Streiffer, L. Q. Chen, S. W. Kirchoefer, J. Levy, and D. G. Schlom, Nature **430**, 758 (2004).
[9] D. Xue, J. Gao, L. Zhang, H. Bao, W. Liu, C. Zhou, and X. Ren, Appl. Phys. Lett. **94**, 082902 (2009).
[10] E. K. H. Salje, *Phase Transitions in Ferroelastic and Co-Elastic Crystals*, Cambridge Topics I (Cambridge University Press, 1993).
[11] N. Barrett, J. Dionot, D. Martinotti, E. K. H. Salje, and C. Mathieu, Appl. Phys. Lett. **113**, 022901 (2018).
[12] F. J. Pérez-Reche, E. Vives, L. Mañosa, and A. Planes, Phys. Rev. Lett. **87**, 195701 (2001).

[13]F.-J. Pérez-Reche, B. Tadić, L. Mañosa, A. Planes, and E. Vives, Phys. Rev. Lett. **93**, 195701 (2004).

[14]E. K. H. Salje and K. A. Dahmen, Annu. Rev. Condens. Matter Phys. **5**, 233 (2014).

[15]E. Vives, J. Baró, M. C. Gallardo, J.-M. Martín-Olalla, F. J. Romero, S. L. Driver, M. A. Carpenter, E. K. H. Salje, M. Stipcich, R. Romero, and A. Planes, Phys. Rev. B **94**, 024102 (2016).

[16]B. Gutenberg, *Seismicity of the Earth and Associated Phenomena* (Read Books Limited, 2013).

[17]F. F. Csikor, C. Motz, D. Weygand, M. Zaiser, and S. Zapperi, Science **318**, 251 (2007).

[18]K. A. Dahmen, Y. Ben-Zion, and J. T. Uhl, Phys. Rev. Lett. **102**, 175501 (2009).

[19]J. Baró, A. Corral, X. Illa, A. Planes, E. K. H. Salje, W. Schranz, D. E. Soto-Parra, and E. Vives, Phys. Rev. Lett. **110**, 088702 (2013).

[20]M. P. Lilly, P. T. Finley, and R. B. Hallock, Phys. Rev. Lett. **71**, 4186 (1993).

[21]J. P. Sethna, K. Dahmen, S. Kartha, J. A. Krumhansl, B. W. Roberts, and J. D. Shore, Phys. Rev. Lett. **70**, 3347 (1993).

[22]J. P. Sethna, K. A. Dahmen, and C. R. Myers, Nature **410**, 242 (2001).

[23]E. K. H. Salje, D. Xue, X. Ding, K. A. Dahmen, and J. F. Scott, Phys. Rev. Mater. **3**, 014415 (2019).

[24]C. Tan, C. Flannigan, J. Gardner, F. Morrison, E. K. H. Salje, and J. Scott, Phys. Rev. Mater. **3**, 034402 (2019).

[25]E. Vives, J. Ortín, L. Mañosa, I. Ràfols, R. Pérez-Magrané, and A. Planes, Phys. Rev. Lett. **72**, 1694 (1994).

[26]E. Vives, D. Soto-Parra, L. Mañosa, R. Romero, and A. Planes, Phys. Rev. B **80**, 180101 (2009).

[27]H. Bauke, Eur. Phys. J. B **58**, 167 (2007).

[28]E. Dul'kin, M. Roth, P.-E. Janolin, and B. Dkhil, Phys. Rev. B **73**, 012102 (2006).

[29]E. K. H. Salje, E. Dul'kin, and M. Roth, Appl. Phys. Lett. **106**, 152903 (2015).

[30]E. Dul'kin, J. Zhai, and M. Roth, Phys. Status Solidi B **252**, 2079 (2015).

[31]F. J. Perez-Reche, C. Triguero, G. Zanzotto, and L. Truskinovsky, Phys. Rev. B **94**, 144102 (2016).

[32]M. C. Gallardo, J. Manchado, F. J. Romero, J. del Cerro, E. K. H. Salje, A. Planes, E. Vives, R. Romero, and M. Stipcich, Phys. Rev. B **81**, 174102 (2010).

[33]F. Jona and G. Shirane, *Ferroelectric Crystals*, Dover Books on Engineering (Dover Publications, 1993).

[34]B. Noheda, D. E. Cox, G. Shirane, J. Gao, and Z.-G. Ye, Phys. Rev. B **66**, 054104 (2002).

[35]Y. Zhang, D. Xue, H. Wu, X. Ding, T. Lookman, and X. Ren, Acta Mater. **71**, 176 (2014).

[36]M. LeBlanc, L. Angheluta, K. Dahmen, and N. Goldenfeld, Phys. Rev. E **87**, 022126 (2013).

[37]B. Gutenberg and C. F. Richter, Nature **176**, 795 (1955).

[38]A. Clauset, C. Shalizi, and M. Newman, SIAM Rev. **51**, 661 (2009).

[39]P. Bak, K. Christensen, L. Danon, and T. Scanlon, Phys. Rev. Lett. **88**, 178501 (2002).

[40]Á. Corral, Physica A **340**, 590 (2004).

[41]D. Sornette and G. Ouillon, Phys. Rev. Lett. **94**, 038501 (2005).

[42]X. Jiang, D. Jiang, J. Chen, and E. K. H. Salje, Am. Mineral. **101**, 2751 (2016).